Appl Phys A (2011) 102: 301–308
DOI 10.1007/s00339-010-5995-3

Applied Physics A
Materials Science & Processing

Vibration of ZnO nanotubes: a molecular mechanics approach

R. Chowdhury · S. Adhikari · F. Scarpa

Received: 25 March 2010 / Accepted: 23 July 2010 / Published online: 17 August 2010

Abstract We investigate the vibrational properties of two kinds of single-wall ZnO nanotubes. The simulations are carried out for three types of zigzag nanotubes $(5, 0)$, $(8, 0)$, $(10, 0)$ and armchair nanotubes $(3, 3)$, $(4, 4)$, $(6, 6)$. The natural frequencies are determined by means of the molecular mechanics approach with the universal force field potential. The first four natural frequencies are obtained for length/diameter ratio of about 5–20. The vibration modes associated with these frequencies have been computed. Closed-form analytical expressions have been derived using the continuum shell theory for the physical explanations of the simulations results. We observe that the natural frequencies decrease as the aspect ratios increase. The results follow similar trends with results of previous studies for carbon nanotubes (CNT). However, the magnitudes of the frequencies are lower from the corresponding CNT counterparts, indicating that ZnO nanotubes are comparatively less stiff.

Keywords Vibrational analysis · ZnO nanotube · Molecular mechanics

R. Chowdhury (✉) · S. Adhikari
Multidisciplinary Nanotechnology Centre, Swansea University, Singleton Park, Swansea SA2 8PP, UK
e-mail: R.Chowdhury@Swansea.ac.uk
Fax: +44-1792-295676

S. Adhikari
e-mail: S.Adhikari@Swansea.ac.uk

F. Scarpa
Advanced Composites Centre for Innovation and Science, University of Bristol, Bristol BS8 1TR, UK
e-mail: F.Scarpa@bris.ac.uk

1 Introduction

Zinc oxide (ZnO) [1] nano materials have attracted extensive attention due of their excellent performance in electronic, ferroelectric, piezoelectric [2] and optical applications [3, 4]. With a band gap in the (∼3.37 eV) range [5, 6] and a large exciton binding energy (∼60 meV) at room temperature, ZnO [7] has many potential advantages in ultraviolet optoelectronic devices. It can be used in the fields of blue and ultraviolet lasers, light-emitting diodes, and solar cells [3, 8]. In recent years, a great variety of ZnO nanostructures was being synthesized [9, 10], and their structural [11, 12], mechanical [13, 14], optical and electrical [15, 16] properties have been investigated experimentally [17, 18]. With regards to the mechanical properties [19, 20], it was found that the bending moduli of ZnO nanobelts are dependent of the aspect ratio in the growth direction [21–23], whereas it is independent of their surface-to-volume ratio [14]. For ZnO nanowires [24], Young' moduli [25] increase with decreasing diameter of the wire, and the values of these Young' moduli were all larger than the bulk value. On the theoretical side, the surface stress induced internal compressive stress played an important role in the change of the Young' modulus [26, 27].

Multiwalled ZnO nanotubes are being synthesized [24, 28, 29]. These tubes are typically 20–450 nm in diameter and wall thicknesses of about 4–100 nm. However, single-walled ZnO nanotubes have not been reported experimentally yet, although the properties of single-walled ZnO nanotubes are simulated [2, 4, 6, 30–33]. ZnO nanotubes are faceted and can be regarded as nanowires with hollow interior centers that preserve the bulk-like configuration. It is found that, resembling carbon or boron-nitride nanotubes, ZnO nanotubes may stably exist due to their negative binding energy. Recently Shen et al. [24] showed that the single-walled ZnO nanotubes are energetically more stable at the

small size. Issues on the stability of ZnO nanotubes are further explored in [29, 34] for their potential applications. In particular, one-dimensional ZnO nanostructures (nanowires, nanorods, nanotubes, etc.) have unique physical and chemical properties arising from the surface and quantum confinement effects. Thus, these nanostructures can be utilized as the fundamental building blocks for field-effect transistors, field emitters, cantilevers, resonators, transducers, sensors and actuators. Investigation and understanding of the vibrating properties are valuable for their potential application in nanomechanical resonators. To the best of our knowledge, there are no theoretical reports about the vibrational properties of single-walled ZnO nanotubes. This study explores the use of ZnO nanotubes as a potential application to vibration-based sensors. A molecular mechanics-based approach is used to estimate the frequencies. In this study, we used the universal force field (UFF) model, wherein the force field parameters are estimated using general rules based only on the element, its hybridization, and its connectivity. The resonance frequencies are calculated for three types of zigzag nanotubes $(5,0)$, $(8,0)$, $(10,0)$ and armchair nanotubes $(3,3)$, $(4,4)$, $(6,6)$ and for different lengths. The values of the resonance frequencies are compared with those from equivalent carbon nanotubes (CNT) [35–38]. Closed-form analytical expressions have been derived using the continuum shell theory for the physical explanations of the simulations results.

2 Structure of single-wall ZnO nanotube

Recently, ZnO nanostructures, specifically nanowires [24] and nanobelts, have been extensively studied because of their potential applications. In contrast, limited works on ZnO nanotubes are reported [34, 39, 40]. Particularly, it seems hard to obtain the tubular structure of the ZnO material as no layered ZnO exists [39]. The hollow 1D ZnO structure could provide more prominent advantages than other 1D ZnO materials like nanowires and nanobelts. Several groups have synthesized hexagonal ZnO nanotubes [41, 42], though single-walled ZnO nanotubes with a round wall have not been realized. A recent study [2] indicated the possibility of synthesizing single-walled ZnO nanotubes [4]. The conventional single-walled ZnO nanotube models (refer to Fig. 1) are created in analogy with single-walled boron-nitride nanotubes. Both zigzag and armchair nanotubes are studied here, although atomic arrangements of zigzag nanotubes are much closer to wurtzite ZnO and are more stable than armchair ones [43]. Equilibrium configurations are obtained for finite length tubes without considering the periodic boundary condition. The optimized equilibrium configurations of the zigzag $(n,0)$ ZnO nanotubes with $n=5,8$ and 10 and the armchair (n,n) ZnO nanotubes with $n=3,4$ and 6 are considered in this vibration analysis. The geometry optimizations were performed with nanotubes rolled up from a graphitic ZnO single layer. The optimized bond length of Zn–O is found to be 1.877 Å [44], which is shorter than the bond length of 1.992 Å in wurtzite ZnO crystal. The average bond angle of $\angle$ Zn–O–Zn and $\angle$ O–Zn–O of the optimized tube is found 118.57°.

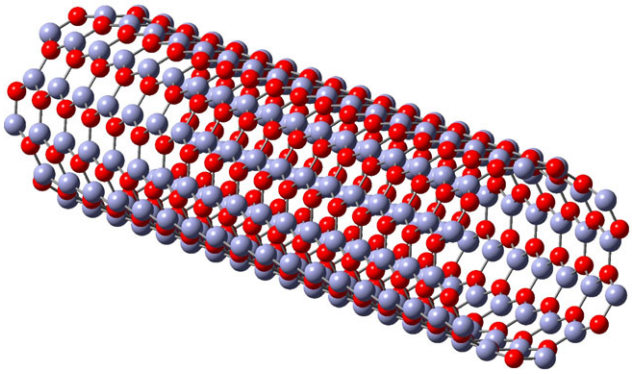

Fig. 1 Atomistic model of a (6,6) ZnO nanotubes with length 58.52 Å and diameter 10.75 Å. *Red* and *gray balls* denote O and Zn atoms, respectively

3 The computational framework

The general expression of the total energy is a sum of energies due to the valence or bonded interactions and non-bonded interactions

$$\begin{aligned} E = {} & \sum k_1(r-r_0)^2 + \sum k_2(C_0 + C_1\cos\theta + C_2\cos 2\theta) \\ & + \sum k_3(1 \pm \cos n\phi) + \sum k_4(1 \pm \cos(n\chi - \chi_0)) \\ & + \sum D\left[\left(\frac{r^*}{r}\right)^{12} - 2\left(\frac{r^*}{r}\right)^{6}\right] + \sum \frac{q_i q_j}{\varepsilon r_{ij}}. \end{aligned} \tag{1}$$

The Fourier coefficients C_0, C_1 and C_2 of the general angle terms are evaluated as a function of the natural bond angle θ_0:

$$\begin{aligned} C_2 &= \frac{1}{4\sin^2\theta_0}, \\ C_1 &= -4C_2\cos\theta_0, \\ C_0 &= C_2(2\cos^2\theta_0 + 1). \end{aligned} \tag{2}$$

Here k_1, k_2, k_3 and k_4 are force constants, D is the van der Waals well depth, r^* is the van der Waals length, q_i is the net charge of an atom, ε is the dielectric constant, r_{ij} is the distance between two atoms. In this study, we used the UFF model [45], wherein the force field parameters are estimated using general rules based only on the element, its hybridization and its connectivity. The force field functional

Table 1 The force field parameters used in the computational method

Atom type	Atomic bond radius (Å)	GMP electro-negativity	Valance		Non-bond		Effective charge
			Bond (Å)	Angle (deg)	Distance (Å)	Energy (Kcal/mol)	
Zn	1.193	5.106	1.193	109.47	2.763	0.124	1.308
O	0.634	8.741	0.634	120.00	3.500	0.060	2.300

forms and parameters used in this study are in accordance with [45]. In Table 1 we provide the force field parameters used in the analysis. In the following section we provide the methodology of the frequency calculation.

3.1 Calculation of the frequencies

We start with the Hessian matrix $\mathbf{f}_{\mathrm{CAR}}$, which holds the second partial derivatives of the potential E with respect to displacement of the atoms in Cartesian coordinates (CAR) [46]:

$$f_{\mathrm{CAR}_{ij}} = \left(\frac{\partial^2 E}{\partial \xi_i \partial \xi_j}\right)_{\mathrm{Opt}}. \tag{3}$$

This is a $3N \times 3N$ matrix (N is the number of atoms), where $\xi_1, \xi_2, \xi_3, \ldots, \xi_{3N}$ are used for the displacements in Cartesian coordinates, $\Delta x_1, \Delta y_1, \Delta z_1, \ldots, \Delta z_N$. The $()_{\mathrm{Opt}}$ refers to the fact that the derivatives are taken at the equilibrium positions of the atoms. These force constants are then converted to mass weighted Cartesian coordinates (MWC) [46]:

$$f_{\mathrm{MWC}_{ij}} = \frac{f_{\mathrm{CAR}_{ij}}}{\sqrt{m_i m_j}} = \left(\frac{\partial^2 E}{\partial q_i \partial q_j}\right)_{\mathrm{Opt}}, \tag{4}$$

where $q_1 = \sqrt{m_1}\xi_1 = \sqrt{m_1}\Delta x_1$, $q_2 = \sqrt{m_1}\xi_2 = \sqrt{m_1}\Delta y_1$ and so on. $\mathbf{f}_{\mathrm{MWC}}$ is diagonalized, yielding a set of $3N$ eigenvectors and $3N$ eigenvalues.

The next step is to translate the center of mass to the origin, and determine the moments and products of inertia, with the goal of finding the matrix that diagonalizes the moment of inertia tensor. Using this matrix we can find the vectors corresponding to the rotations and translations. Once these vectors are known, we know that the rest of the normal modes are vibrations. The center of mass $\mathbf{R}_{\mathrm{COM}}$ is found in the usual way:

$$\mathbf{R}_{\mathrm{COM}} = \frac{\sum_\alpha m_\alpha \mathbf{r}_\alpha}{\sum_\alpha m_\alpha}, \tag{5}$$

where the sums are over the atoms, α. The origin is then shifted to the center of mass $\mathbf{r}_{\mathrm{COM}_\alpha} = \mathbf{r}_\alpha - \mathbf{R}_{\mathrm{COM}}$. Next we have to calculate the moments of inertia (the diagonal elements) and the products of inertia (off diagonal elements) of the moment of inertia tensor ($\mathbf{I}$).

$$\mathbf{I} = \begin{Bmatrix} I_{xx} & I_{xy} & I_{xz} \\ I_{yx} & I_{yy} & I_{yz} \\ I_{zx} & I_{zy} & I_{zz} \end{Bmatrix} = \begin{Bmatrix} \sum_\alpha m_\alpha (y_\alpha^2 + z_\alpha^2) & -\sum_\alpha m_\alpha (x_\alpha y_\alpha) & -\sum_\alpha m_\alpha (x_\alpha z_\alpha) \\ -\sum_\alpha m_\alpha (y_\alpha x_\alpha) & \sum_\alpha m_\alpha (x_\alpha^2 + z_\alpha^2) & -\sum_\alpha m_\alpha (y_\alpha z_\alpha) \\ -\sum_\alpha m_\alpha (z_\alpha x_\alpha) & -\sum_\alpha m_\alpha (z_\alpha y_\alpha) & \sum_\alpha m_\alpha (x_\alpha^2 + x_\alpha^2) \end{Bmatrix}. \tag{6}$$

This symmetric matrix is diagonalized, yielding the principal moments (the eigenvalues $\mathbf{I}'$) and a 3×3 matrix (X), which is made up of the normalized eigenvectors of ($\mathbf{I}$). The eigenvectors of the moment of inertia tensor are used to generate the vectors corresponding to translation and infinitesimal rotation of the molecular system. A Schmidt orthogonalization is used to generate $N_{\mathrm{vib}} = 3N - 6$ remaining vectors, which are orthogonal to the six rotational and translational vectors. The result is a transformation matrix $\mathbf{D}$ which transforms from mass weighted Cartesian coordinates $\mathbf{q}$ to internal coordinates $\mathbf{S} = \mathbf{Dq}$, where rotation and translation have been separated out. Now that we have coordinates in the rotating and translating frame, we need to transform the Hessian, $\mathbf{f}_{\mathrm{MWC}}$, to these new internal coordinates (INT) [46]. Only the N_{vib} coordinates corresponding to internal coordinates will be diagonalized, although the full $3N$ coordinates are used to transform the Hessian. The transformation is straightforward as follows:

$$\mathbf{f}_{\mathrm{INT}} = \mathbf{D}^T \mathbf{f}_{\mathrm{MWC}} \mathbf{D}. \tag{7}$$

The $N_{\mathrm{vib}} \times N_{\mathrm{vib}}$ submatrix of $\mathbf{f}_{\mathrm{INT}}$, which represents the force constants internal coordinates, is diagonalized yielding N_{vib} eigenvalues $\lambda = 4\pi^2\omega^2$, and N_{vib} eigenvectors. If we call the transformation matrix composed of the eigenvectors $\mathbf{L}$, then we have

$$\mathbf{L}^T \mathbf{f}_{\mathrm{INT}} \mathbf{L} = \Lambda, \tag{8}$$

where Λ is the diagonal matrix with eigenvalues λ_i. At this point, the eigenvalues need to be converted frequencies:

$$\omega_i = \sqrt{\frac{\lambda_i}{4\pi^2}}. \tag{9}$$

In the context of CNT, the calculation of resonance frequencies using this approach and its validation can be found in [47].

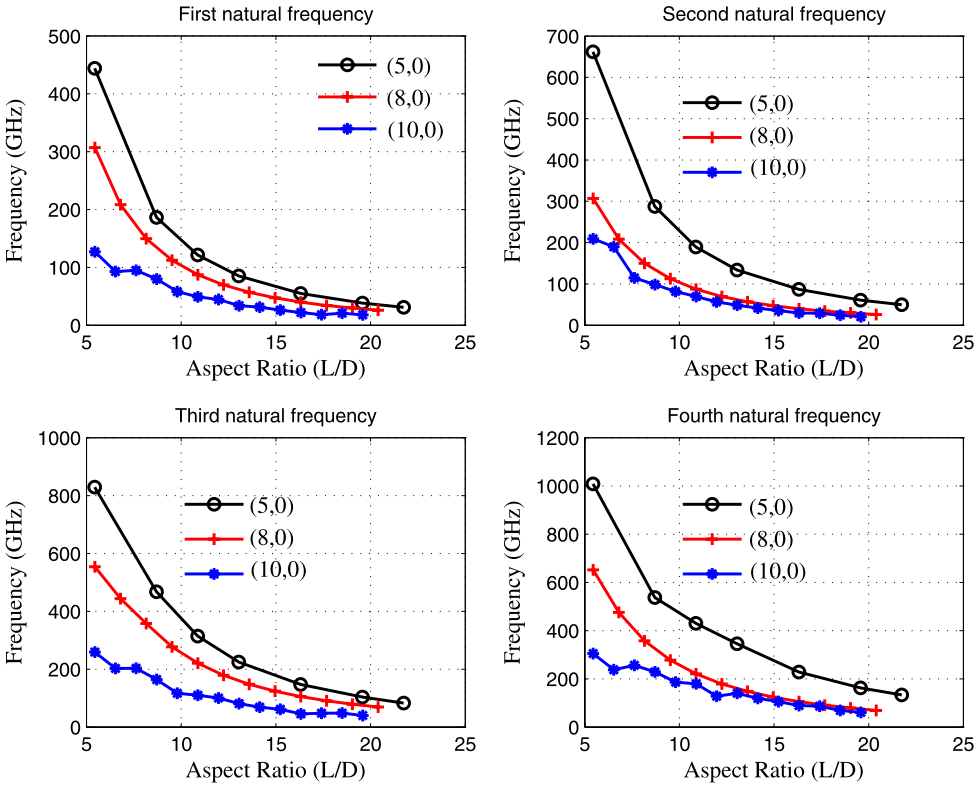

Fig. 2 The first four vibrational frequencies of zigzag ZnO nanotube as a function of tube aspect ratio (L/D). The first three modes correspond to different bending modes and torsional modes are observed for the fourth frequency

4 Results and discussion

The resonant frequencies of nanotubes-based resonators depend on the tube diameter and length. In this work, we analyze two forms of nanotube resonators, i.e., three types of zigzag nanotubes $(5,0)$, $(8,0)$, $(10,0)$ and armchair nanotubes $(3,3)$, $(4,4)$, $(6,6)$. The computational results of the first four vibrational frequencies of the single-walled zigzag and armchair ZnO nanotube resonators are shown in Fig. 2 and Fig. 3, respectively.

For nanotubes with length/diameter ratios of about 5–20, the fundamental frequencies are in the ranges of about 125–450 GHz and about 170–525 GHz, respectively, for zigzag and armchair nanotubes. For both type of nanotubes, the frequencies decrease with the increasing aspect ratios. For the same aspect ratio, nanotubes with a smaller diameter have higher frequencies. The effect of tube chirality on the fundamental frequency is in the range of several giga Hertz. In general, frequencies are in decreasing trend with the increasing aspect ratio. It can be observed from the figures that, for the case of $(8,0)$ (ref. Fig. 2) and $(3,3)$ and $(4,4)$ (refer to Fig. 3), first and second frequencies are identical. This is due to the fact that both the modes correspond to bending modes with different symmetric planes of vibration.

A first-order shell model is used to predict the vibration of cylindrical shells in the bending deformation [48]. For modes with m half-wave numbers and no circumferential (ring) waves ($n = 0$), the natural frequency of a cylindrical shell with diameter D, thickness h and length L can be expressed as

$$\omega_m^2 = \frac{E}{3\rho(1-\nu)^2}\left(\frac{2h}{D}\right)^2 \frac{1}{D^2}\left[\left(\frac{m\pi D}{2L}\right)^2 - 1\right]\left(\frac{m\pi D}{2L}\right)^2. \tag{10}$$

Let us consider the case where different tubes having the same diameter D_0 but different length L are considered. The natural frequency ω_{0m} will correspond to a specific tube having diameter and length D_0 and L_0 respectively, and longitudinal half-wave number m. The ratio of the natural frequency ω_m corresponding to the tube with diameter D_0 and different length L, and the frequency ω_{0m} (diameter D_0 and length L_0) can be obtained from (10) as

$$\frac{\omega_m}{\omega_{0m}} = \left(\frac{L_0}{L}\right)^2 \sqrt{\frac{m^2\pi^2 D_0^2 - 4L^2}{m^2\pi^2 D_0^2 - 4L_0^2}}. \tag{11}$$

For higher wavenumbers ($m \to \infty$), the above equation simplifies to $(L_0/L)^2$. Equation (11) is valid for shells made of transversely isotropic material—i.e., with a flexural stiffness $D_f = E\,h^3/12/(1-\nu^2)$, where E is the Young modulus of the materials, h the thickness of the shell and ν is the Poisson ratio of the core material [48].

Figure 4 shows the distribution of the frequency ratio ω_m/ω_{0m} for the first 3 bending modes. A linear least square

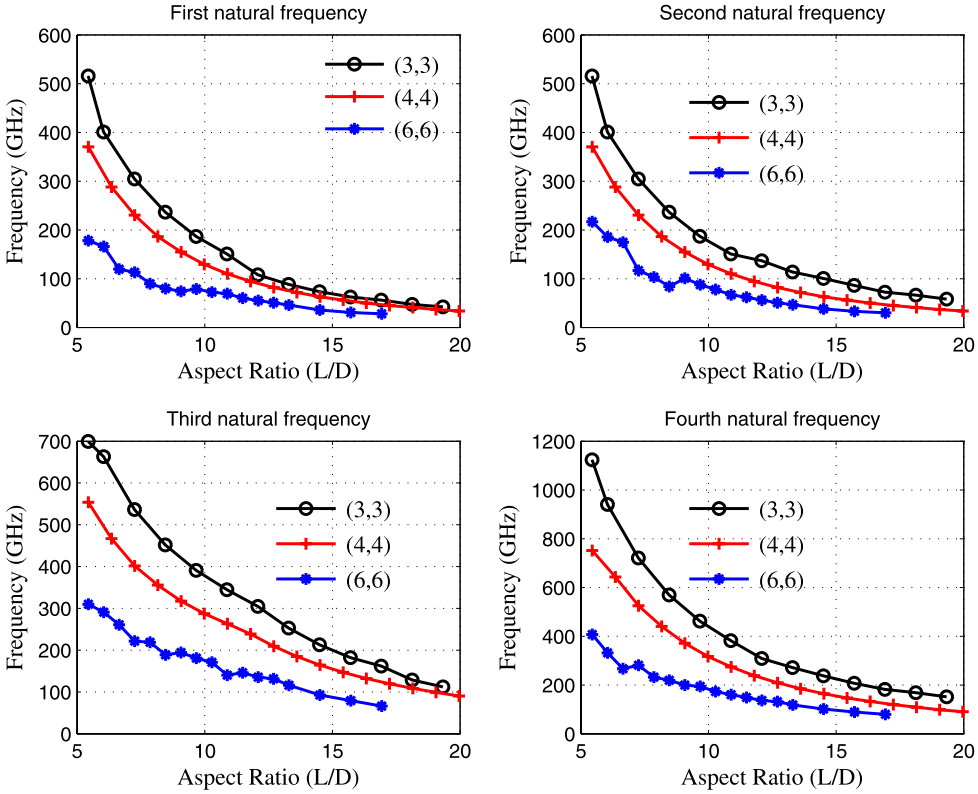

Fig. 3 The first four vibrational frequencies of armchair ZnO nanotube as a function of tube aspect ratio (L/D). Similar to zigzag nanotubes, the first three modes correspond to different bending modes, and torsional modes are observed for the fourth frequency. But the frequencies observed in this case are higher than zigzag nanotubes

(LLS) fit of the frequency data versus $(L_0/L)^2$ provides a linear curve with $R^2 = 0.966$ of the type $\omega_m/\omega_{0m} \approx p_1(L_0/L)^2 + p_2$, where $p_1 = 0.965$ and $p_2 = 0.064$, with both coefficients having a confidence level of 95%. It appears that all nanotubes show a stiffening effect over the bending-dominated deformation, with a contribution from membrane effects [48]. The departure from the linear dependence over $(L_0/L)^2$ seems more significant for the higher radius tubes ($(8, 0)$ and $(10, 0)$). The bending-membrane coupling is likely to occur in anisotropic tubular grid-like structures, with different radial and tangential stiffnesses based on the lattice topology (chirality) of the tube, and the diameter of the tubular structure itself [49]. Jeong and Ruzzene [50] have identified strong directional acoustic signature and different modal density distributions for anisotropic tubular grid-like structures compared to transversely isotropic systems. The distribution of bond lengths and internal angles at equilibrium suggest different transverse and radial stiffness, making (11) indicative in terms of trends.

Under the Love equations' approximation, the natural frequencies related to the torsional modes of cylindrical shells can be assimilated to the vibrational behavior of circular torsional bars [48]. The mth fundamental resonant frequency for a bar in torsion having length L and uniform cross-section can be expressed as:

$$\omega_m = m\frac{c}{L}, \tag{12}$$

where $c = \sqrt{G/\rho}$, G being the shear modulus and ρ the density of the material. Similarly to the bending mode case (4), we can consider for the same half-wave number the ratio between two torsional rods, having the same cross section, but different lengths (L_0 and L). The scaling of the torsional modes versus the length of the tube can therefore be represented as:

$$\frac{\omega_{tn}}{\omega_{tn0}} = \frac{L_0}{L}. \tag{13}$$

LLS fit of the torsional frequencies provides a curve of the type $\omega_{tn}/\omega_{tn0} \approx c_1(L_0/L) + c_2$, where $c_1 = 1.165$ and $c_2 = -0.147$ (Fig. 5). The coefficients (all within a confidence interval of 95%) and the fit have a $R^2 = 0.914$. Similarly to the bending-dominated modes, we observe a departure from the linear scaling over L_0/L, suggesting again a complex shear pattern affected by coupling between the shear and membrane stiffnesses, like in anisotropic cellular shell structures [50]. The smaller tubes $(5, 0)$ appear to be less affected by the membrane coupling and possible transverse shear deformation effects [48].

A significant amount of studies on the vibration of CNT resonators (see for example [35–38]) is available in the literature. Therefore, it may useful to relate the new results obtained here for the ZnO nanotube resonators with the equivalent results from CNT resonators. The comparisons of the first-mode frequencies of ZnO nanotubes with CNTs are shown in Fig. 6. The same computational methodology is

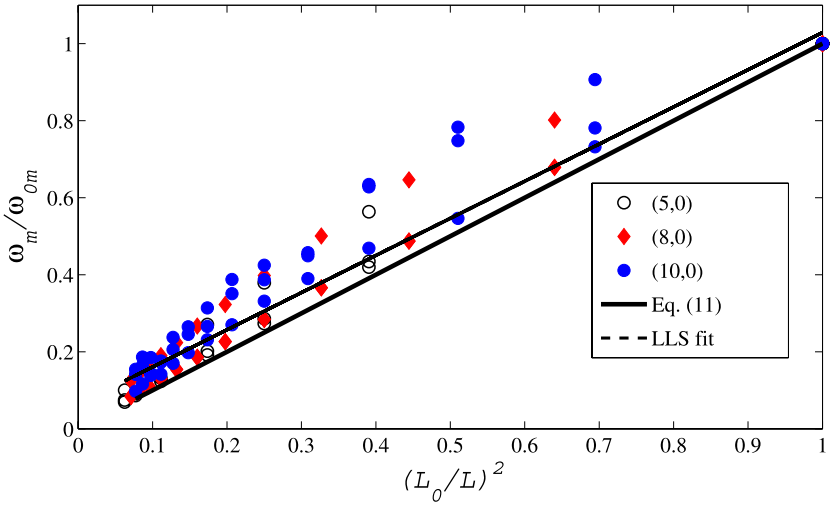

Fig. 4 The distribution of ω_m/ω_{0m} for the first three bending modes of $(5, 0)$, $(8, 0)$ and $(10, 0)$ ZnO tubes. For a given nanotube, all the three bending modes are marked with the same marker. For a fixed value of $(L_0/L)^2$, the top point is the lowest mode and the bottom point is the highest mode. The linear least square (LLS) fit of the frequency data versus $(L_0/L)^2$ provides the expression $\omega_m/\omega_{0m} \approx p_1(L_0/L)^2 + p_2$, where $p_1 = 0.965$ and $p_2 = 0.064$. The membrane-bending coupling stiffening effect due to anisotropy of the lattice appears evident in medium and higher order bending modes for $(L_0/L)^2 > 0.2$

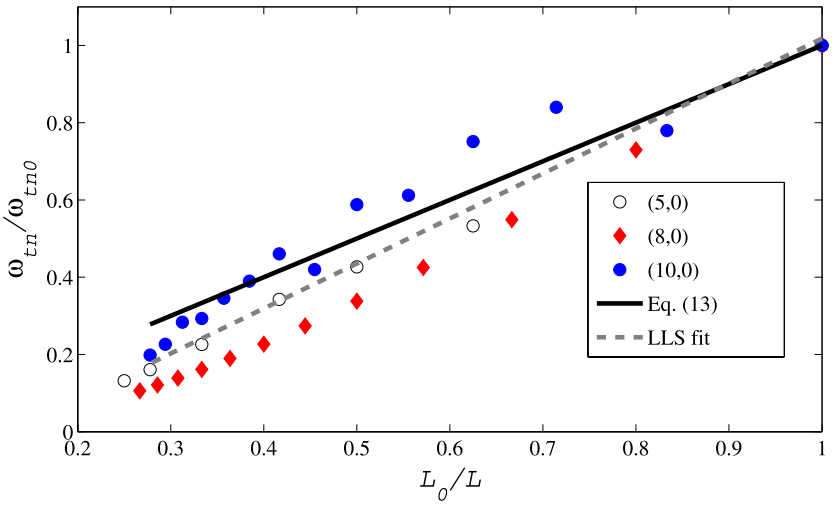

Fig. 5 The dependence of the torsional frequency ratio versus L_0/L. The linear least square (LLS) fit of the frequency data versus (L_0/L) provides an expression $\omega_{tn}/\omega_{tn0} \approx c_1(L_0/L) + c_2$, where $c_1 = 1.165$ and $c_2 = -0.147$. The torsional dynamic stiffness appears to be decreased for $(8, 0)$ and $(5, 0)$ configurations, while the higher radius tubes follow more closely the trend of (13)

used to obtain the frequencies of the CNT resonators. Two atomic configurations, namely $(5, 0)$ and $(4, 4)$, are considered for illustration. The frequencies of the CNT are significantly higher compared to the equivalent ZnO nanotubes for small values of the aspect ratio. For higher values of the aspect ratio, the difference between the frequencies reduces as the length of the nanotube increases. In order to explain this, we note that the resonant frequency of an elastic cylindrical shell is

$$\omega \propto \frac{1}{L^2}\sqrt{\frac{D_f}{\rho}}, \tag{14}$$

where D_f is the flexural stiffness of the structure, ρ the mass density per unit length of the core material and L is the length of the shell. Using (14), the difference in the frequencies of CNT and ZnO nanotubes with identical length can be expressed as

$$\omega_{\text{CNT}} - \omega_{\text{ZnO}} \propto \frac{1}{L^2}\left(\sqrt{\frac{E_{\text{CNT}}}{\rho_{\text{CNT}}}} - \sqrt{\frac{E_{\text{ZnO}}}{\rho_{\text{ZnO}}}}\right), \tag{15}$$

where E_{CNT} and E_{ZnO} are defined as the Young moduli of CNT and ZnO, respectively. From this equation, it can be observed that the difference in the frequencies is inversely proportional to the square of the length of the tube for a particular atomic configuration. Due to this fact, the differences in the magnitude of the frequencies between CNT and ZnO nanotubes are decreasing with the increase in the aspect ratio in Fig. 6.

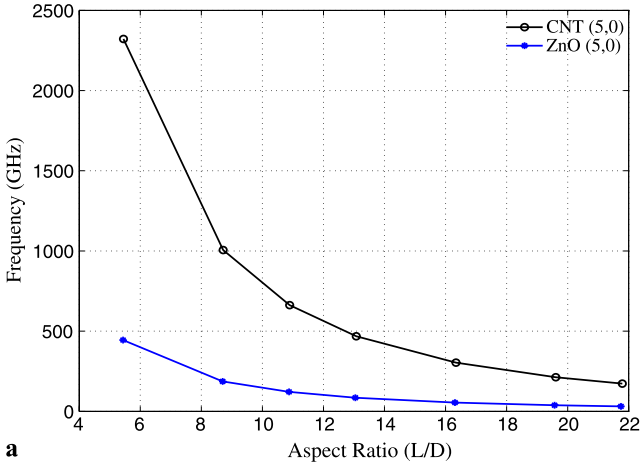

Comparison of the first-mode frequencies of (5,0) nanotubes for different aspect ratios.

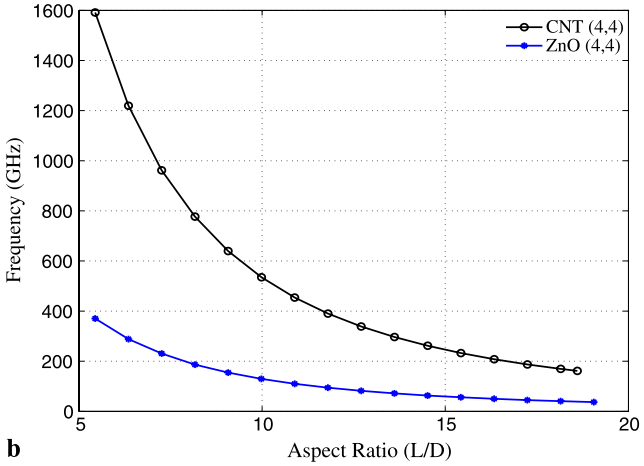

Comparison of first-mode frequencies of (4,4) nanotubes for different aspect ratios.

Fig. 6 The comparison of the first-mode frequencies of ZnO nanotubes with CNTs. Two atomic configurations, namely $(5, 0)$ and $(4, 4)$, are considered for illustration. The frequencies of the CNT are significantly higher compared to ZnO nanotubes for small values of the aspect ratio. For higher values of the aspect ratio, the difference between the frequencies reduces as the length of the nanotube increases

Another issue relevant to nanomechanical resonators is the vibrational mode associated with the frequencies. It is found that the first, and even the second and third, vibration modes are in the shape of a half sine wave with bending about different axes. However, higher modes correspond to torsional, axial and mixed modes. For the illustration purpose, the modes of vibration of $(5, 0)$ with aspect ratio 8.71 and $(4, 4)$ with aspect ratio 7.26 are provided in the supporting document.

5 Conclusions

The vibrational properties of two kinds of single-walled ZnO nanotubes (zigzag and armchair) are studied. The optimized bond length and bond angle are found to be 1.877 Å and 118.57° respectively. Results indicate that natural frequencies of ZnO nanotubes are lower compared to their corresponding CNT counterparts. This indicates that ZnO nanotubes are more flexible compared to corresponding CNT. The vibration of the ZnO nanotube shows similar features of decreasing frequencies with the increase in aspect ratio. The general trends in the variation of the frequencies have been explained using simple closed-form expressions derived using the homogeneous continuum theory. From the results reported in the paper, likewise CNT-based nanoresonators, nanomechanical resonators can be achieved using single-walled ZnO nanotubes. The primary advantage of using ZnO-based nanoresonator can be realized for promising biosensor due to biosafety and bio-compatibility. Future study is necessary aimed at the thermal effect and coupled electro-mechanical analysis.

Acknowledgements RC acknowledges the support of Royal Society through the award of Newton International Fellowship. SA gratefully acknowledges the support of the Leverhulme Trust for the award of the Philip Leverhulme Prize. FS acknowledges the support of the FP6 STRP01364 CHISMACOMB project for the CPU time.

References

1. U. Ozgur, Y. Alivov, C. Liu, A. Teke, M. Reshchikov, S. Dogan, V. Avrutin, S. Cho, H. Morkoc, J. Appl. Phys. **98**(4), 041301 (2005)
2. Z.C. Tu, X. Hu, Phys. Rev. B **74**(3), 035434 (2006)
3. D. Look, D. Reynolds, J. Sizelove, R. Jones, C. Litton, G. Cantwell, W. Harsch, Solid State Commun. **105**(6), 399 (1998)
4. Z. Fu-Chun, Z. Zhi-Yong, Z. Wei-Hu, Y. Jun-Feng, Y. Jiang-Ni, Chin. Phys. Lett. **26**(1), 016105 (2009)
5. Q. Wan, Z. Xiong, J. Dai, J. Rao, F. Jiang, Opt. Mater. **30**, 817 (2008)
6. Y. Yu-Rong, Y. Xiao-Hong, G. Zhao-Hui, D. Yu-Xiang, Chin. Phys. B **17**(9), 3433 (2008)
7. F. Decremps, F. Datchi, A. Saitta, A. Polian, S. Pascarelli, A. Di Cicco, J. Itie, F. Baudelet, Phys. Rev. B **68**(10), 104101 (2003)
8. Z. Tang, G. Wong, P. Yu, M. Kawasaki, A. Ohtomo, H. Koinuma, Y. Segawa, Appl. Phys. Lett. **72**(25), 3270 (1998)
9. Z. Wang, J. Phys. Condens. Matter **16**(25), R829 (2004)
10. Y. Sun, D.J. Riley, M.N.R. Ashfold, J. Phys. Chem. B **110**(31), 15186 (2006)
11. X.J. Liu, J.W. Li, Z.F. Zhou, L.W. Yang, Z.S. Ma, G.F. Xie, Y. Pan, C.Q. Sun, Appl. Phys. Lett. **94**(13), 131902 (2009)
12. W.F. Perger, J. Criswell, B. Civalleri, R. Dovesi, Comput. Phys. Commun. **180**(10), 1753 (2009)
13. J. Qi, D. Shi, B. Wang, Comput. Mater. Sci. **46**(2), 303 (2009)
14. H. Ni, X. Li, Nanotechnology **17**(14), 3591 (2006)
15. M. Arnold, P. Avouris, Z. Pan, Z. Wang, J. Phys. Chem. B **107**(3), 659 (2003)
16. R. Zhu, D. Wang, S. Xiang, Z. Zhou, X. Ye, Sens. Actuators A **154**(2), 224 (2009). Special Issue

17. A. Asthana, K. Momeni, A. Prasad, Y.K. Yap, R.S. Yassar, Appl. Phys. Lett. **95**(17), 172106 (2009)
18. R. Agrawal, H.D. Espinosa, J. Eng. Mater. Technol., Trans. ASME **131**(4), 041208 (2009)
19. A.V. Desai, M.A. Haque, Sens. Actuators A **134**(1), 169 (2007). Special Issue
20. M. Riaz, O. Nur, M. Willander, P. Klason, Appl. Phys. Lett. **92**(10), 034309 (2008)
21. M. Lucas, W. Mai, R. Yang, Z.L. Wang, E. Riedo, Nano Lett. **7**(5), 1314 (2007)
22. W. Mai, Z.L. Wang, Appl. Phys. Lett. **89**(7), 073112 (2006)
23. X. Bai, P. Gao, Z. Wang, E. Wang, Appl. Phys. Lett. **82**(26), 4806 (2003)
24. X. Shen, P.B. Allen, J.T. Muckerman, J.W. Davenport, J.C. Zheng, Nano Lett. **7**(8), 2267 (2007)
25. C. Chen, Y. Shi, Y. Zhang, J. Zhu, Y. Yan, Phys. Rev. Lett. **96**(7), 075505 (2006)
26. A. Kulkarni, M. Zhou, F. Ke, Nanotechnology **16**(12), 2749 (2005)
27. A.J. Kulkarni, M. Zhou, Acta Mech. Sin. **22**(3), 217 (2006)
28. Y. Sun, G. Fuge, N. Fox, D. Riley, M. Ashfold, Adv. Mater. **17**(20), 2477 (2005)
29. H. Li, Z.H. Jiang, Q. Jiang, Chem. Phys. Lett. **465**(1–3), 78 (2008)
30. S. Erkoc, H. Kokten, Phys. E-Low-Dimens. Syst. Nanostruct. **28**(2), 162 (2005)
31. Z. Fan, J. Lu, J. Nanosci. Nanotechnol. **5**(10), 1561 (2005)
32. X. Kong, X. Sun, X. Li, Y. Li, Mater. Chem. Phys. **82**(3), 997 (2003)
33. H. Xu, F. Zhan, A.L. Rosa, T. Frauenheim, R.Q. Zhang, Solid State Commun. **148**(11–12), 534 (2008)
34. Y. Li, Z. Zhou, Y. Chen, Z. Chen, J. Chem. Phys. **130**(20), 204706 (2009)
35. C. Li, T.W. Chou, Int. J. Solids Struct. **40**(10), 2487 (2003)
36. K. Hashemnia, M. Farid, R. Vatankhah, Comput. Mater. Sci. **47**(1), 79 (2009)
37. F. Scarpa, S. Adhikari, J. Non-Cryst. Solids **354**(35–39), 4151 (2008)
38. S.K. Georgantzinos, G.I. Giannopoulos, N.K. Anifantis, Comput. Mech. **43**(6), 731 (2009)
39. H. Xu, R.Q. Zhang, X. Zhang, A.L. Rosa, T. Frauenheim, Nanotechnology **18**(48), 485713 (2007)
40. R. Chowdhury, S. Adhikari, F. Scarpa, Phys. E-Low-Dimens. Syst. Nanostruct. **42**(8), 2036 (2010)
41. Y. Xing, Z. Xi, X. Zhang, J. Song, R. Wang, J. Xu, Z. Xue, D. Yu, Solid State Commun. **129**(10), 671 (2004)
42. A. Wei, X. Sun, C. Xu, Z. Dong, M. Yu, W. Huang, Appl. Phys. Lett. **88**(21), 213102 (2006)
43. Z. Zhou, Y. Li, L. Liu, Y. Chen, S.B. Zhang, Z. Chen, J. Phys. Chem. C **112**(36), 13926 (2008)
44. B. Wang, S. Nagase, J. Zhao, G. Wang, Nanotechnology **18**(34), 345706 (2007)
45. A.K. Rappe, C.J. Casewit, K.S. Colwell, W.A. Goddard, W.M. Skiff, J. Am. Chem. Soc. **114**(25), 10024 (1992)
46. D.F. McIntosh, Theor. Chem. Acc., Theory Comput. Model. **125**(3–6), 177 (2010)
47. R. Chowdhury, S. Adhikari, C.Y. Wang, F. Scarpa, Comput. Mater. Sci. **48**(4), 730 (2010)
48. W. Soedel, *Vibration of Shells and Plates*, 3rd edn. (Marcel Dekker, New York, 2004)
49. F. Scarpa, C.W. Smith, M. Ruzzene, K. Wadee, Phys. Stat. Solidi B **245**(3), 584 (2008)
50. S.M. Jeong, M. Ruzzene, Shock Vib. **11**(3–4), 311 (2004)